State and bias estimation for soil moisture profiles by an ensemble Kalman filter: Effect of assimilation depth and frequency

Gabriëlle J. M. De Lannoy,[1] Paul R. Houser,[2] Valentijn R. N. Pauwels,[1] and Niko E. C. Verhoest[1]

Received 14 April 2006; revised 22 December 2006; accepted 24 January 2007; published 7 June 2007.

[1] An ensemble Kalman filter for state estimation and a bias estimation algorithm were applied to estimate individual soil moisture profiles in a small corn field with the CLM2.0 model through the assimilation of measurements from capacitance probes. Both without and with inclusion of bias correction, the effect of the assimilation frequency, the assimilation depth, and the number of observations assimilated per profile were studied. Assimilation of complete profiles had the highest impact on deeper soil layers, and the optimal assimilation frequency was about 1–2 weeks, if bias correction was applied. The optimal assimilation depth depended on the calibration results. Assimilation in the surface layer had typically less impact than assimilation in other layers. Through bias correction the soil moisture estimate greatly improved. In general, the correct propagation of the innovations for both the bias-blind state and bias filtering from any layer to other layers was insufficient. The approximate estimation of the a priori (bias) error covariance and the choice of a zero-initialized persistent bias model made it impossible to estimate the bias in layers for which no observations were available.

Citation: De Lannoy, G. J. M., P. R. Houser, V. R. N. Pauwels, and N. E. C. Verhoest (2007), State and bias estimation for soil moisture profiles by an ensemble Kalman filter: Effect of assimilation depth and frequency, *Water Resour. Res.*, *43*, W06401, doi:10.1029/2006WR005100.

1. Introduction

[2] The estimation of soil moisture profiles has received considerable attention, because a correct assessment of the soil moisture state is crucial to estimate the partitioning of surface fluxes, for weather predictions and climate analyses [*Dirmeyer*, 2000; *Koster et al.*, 2004]. The combination of observational information with model simulations is generally accepted to be superior for state reconstruction as compared to either source of information separately, as demonstrated by, for example, *Reichle and Koster* [2005].

[3] In data assimilation studies aiming at the estimation of soil moisture, different types of soil moisture observations have been used: synthetic ground data [*Walker et al.*, 2001a], real ground point measurements [*Walker et al.*, 2001b; *Heathman et al.*, 2003], synthetic remote sensing data [*Entekhabi et al.*, 1994; *Hoeben and Troch*, 2000; *Reichle et al.*, 2002a] and real remote sensing data [*Galantowicz et al.*, 1999; *Houser et al.*, 1998; *Crosson et al.*, 2002; *Margulis et al.*, 2002; *Pauwels et al.*, 2002; *Crow and Wood*, 2003]. Also, a wide range of models have been explored to simulate soil moisture, ranging from simple Darcy-based vertical profile representations to complex distributed land surface models, ultimately coupled with climate models or models for numerical weather prediction.

[4] Several authors have shown that the errors in model predictions or in observations (e.g., *Ni-Meister et al.* [2005] for remotely sensed observations and model predictions for soil moisture) may contain systematic components, i.e., bias. *Reichle et al.* [2004] compared three independent surface soil moisture data sets, and found large discrepancies between them, pointing to the need for bias estimation and correction or rescaling, before the combination of data and model information in an assimilation procedure. While proper quality control can reduce bias in observations, it may be impossible to find a system identification procedure that is able to yield a model that is never (temporarily) biased. With shortcomings in the model structure or parameters, using state estimation only may not be adequate. Therefore, in several hydrological studies, the potential of parameter estimation through filtering was investigated [*Hebson and Wood*, 1985; *Boulet et al.*, 2002; *Moradkhani et al.*, 2005; *Vrugt et al.*, 2005], often in combination with state estimation. However, in case of a large number of parameters, it may be better advised to estimate an integrated bias value to correct the model results. *Friedland* [1969] developed a method for bias estimation in a Kalman filter framework. This work was further explored and applied by *Dee and da Silva* [1998] and *Dee and Todling* [2000].

[5] For state estimation by sequential techniques, simple methods as well as more advanced filtering techniques have

[1] Laboratory of Hydrology and Water Management, Ghent University, Ghent, Belgium.
[2] Center for Research on Environment and Water, George Mason University, Calverton, Maryland, USA.

0043-1397/07/2006WR005100$09.00

been used for data assimilation in hydrological applications. *Houser et al.* [1998] indicated that more complex assimilation schemes yielded better results in a 3-D assimilation study, using real data. *Walker et al.* [2001a] found that the (extended) Kalman filter outperformed a simple technique like direct insertion for profile soil moisture estimation. The ensemble Kalman filter (ENKF) [*Evensen*, 2003] was found to be an effective and efficient tool for state estimation in nonlinear models, such as demonstrated in synthetical studies [*Reichle et al.*, 2002a, 2002b; *Crow*, 2003] and field studies [*Margulis et al.*, 2002] on higher dimensional assimilation.

[6] However, Kalman filtering techniques require more computational effort than simple techniques. Similar to simpler methods, they rely on a number of assumptions, such as the correct knowledge of the first- and second-order statistics of the process and measurement noise, which often limit their success in real case studies. An additional challenge for Kalman filters is that the dynamics of these statistics are to be estimated. Therefore, in many studies, idealized or simplified conditions were considered. Several studies have been reported on profile estimation through Kalman filtering of synthetic ground measurements [*Walker et al.*, 2001a] or synthetic brightness or backscatter data, including a more complex observation model [*Entekhabi et al.*, 1994; *Hoeben and Troch*, 2000]. These studies are mostly feasibility studies which circumvent inaccurate knowledge of error covariance matrices and problems of model or observation bias. However, with real data, *Walker et al.* [2001b], for example, found that difficulties occurred because of the presence of model bias, and many shortcomings in assimilation results have been found due to incorrect knowledge of the error covariances. Another simplification is the definition of the soil profile: often the vertical variability is integrated in a few soil layers. This reduces the size of the state and the state error covariance matrix and prohibits a detailed validation. Further, in most of the hydrological 3-D studies, the error covariance matrices have been sparsely filled and horizontal correlations have been neglected [*Reichle and Koster*, 2003], to take advantage of a (block) diagonal structure for the inverse calculation.

[7] For this study, the ENKF was used with the Community Land Model (CLM2.0) to assimilate ground measurements for soil moisture profile estimation. The focus was on the determination of the best observation conditions for assimilation and on the optimization of the method with real data, without an in-depth evaluation of the effect on related state variables or fluxes, such as evapotranspiration or runoff, which will be addressed by G. J. M. De Lannoy et al. (Correcting for forecast bias in soil moisture assimilation with the ensemble Kalman filter, submitted to *Water Resources Research*, 2006, hereinafter referred to as De Lannoy et al., submitted manuscript, 2006). While the ENKF is a very flexible tool for state estimation, several studies showed that the assumption of Gaussian a priori state estimates has often been violated. Perturbation of parameters, forcings and initial states sometimes resulted in skewed [*Reichle et al.*, 2002a; *Crow*, 2003] or biased [*De Lannoy et al.*, 2006a] distributions of the forecasted state estimates. In this work, the correct specification of the first and second moments of forecast error will be shown to be crucial for successful state estimation with an ENKF. Several scenarios for state and bias estimation will be examined for a collection of completely independent single-column assimilation problems.

[8] First, the soil moisture data and the land surface model are discussed in section 2. In section 3, the state and bias estimation with an ENKF are explained. In section 4, several assimilation scenarios are analyzed and the filter performances are discussed in section 5.

2. Data and Model Description

2.1. Data

[9] Soil moisture observations were collected in a 21 ha corn field on which the Optimizing Production Inputs for Economic and Environmental Enhancement (OPE^3, http://hydrolab.arsusda.gov/ope3/) project is conducted. This field is managed by the Beltsville Agricultural Research Center (BARC) of the Agricultural Research Service (ARS) of the U.S. Department of Agriculture (USDA). The site is situated in Prince George's County, Maryland, and it is part of the Anacostia watershed. The four subwatersheds within the field are named A, B, C and D from north to south and in each subwatershed 12 capacitance probes (EnviroSCAN, SENTEK Pty Ltd., South Australia) provide soil moisture data every 10 min. The observations were aggregated into hourly time steps for comparison with model results.

[10] The probes were named following a 3 digit system. The first letter represents the name of the subwatershed (A, B, C, D), the second letter (L, H, M) refers to the estimated infiltration rate at the point of installation (low, high, moderate clay content) and the third digit (1, 2, 3, 4) discerns between the different probes of a specific infiltration regime [*Gish et al.*, 2002]. H probes have sensors at 10, 30, and 80 cm. L and M probes have sensors at 10, 30, 50, 120, 150, and 180 cm. L probes have an additional sensor at 80 cm depth. In this study, data collected from 1 May 2001 through 30 April 2002 were used. During this period 36 out of 48 probes were operational. A detailed analysis of the 4-D soil moisture data set [*De Lannoy et al.*, 2006b] revealed a complex subsurface hydrology, mainly caused by an irregular shaped clay layer at 1 to 3 m depth.

[11] The data from 1 May 2001 through 1 October 2001 were used for system identification (parameter and initial state estimation), while the remaining data from 2 October 2001 through 30 April 2002 served for state estimation and validation.

[12] The meteorological data required to force the land surface model include air temperature [K], wind speed [m/s], specific humidity [kg/kg], incident solar radiation [W/m^2] and total precipitation [mm/s] (other forcings are calculated by the model itself). Three sources of meteorological data were used to generate a continuous time series: (1) a 10 m high USDA meteorological tower in field B, (2) 3.5 m high meteorological tower of the Powder Mill Soil Climate Analysis Network (SCAN) just outside field D, and (3) the 3.05 m high tower at the Station 3 Old Beltsville Airport. The observed forcings were assumed to be spatially uniform over the relatively small area of the OPE^3 field.

2.2. Model Description

[13] The Community Land Model (CLM2.0) simulates land surface processes by calculating water and heat fluxes

and states for each grid cell separately, without any interaction between cells [*Dai et al.*, 2003]. Each grid cell can be subdivided into several patches, containing one single land cover type. Here, each grid cell was completely covered with vegetation. The vegetated fraction is further subdivided into patches of plant functional types [*Bonan et al.*, 2002], which maintain their own prognostic variables. For the model applications in this study, CLM2.0 was adapted such that for each grid cell the individual patches served as ensemble members, i.e., in addition to differences in vegetation parameters, also differences in soil parameters and forcings were included [*De Lannoy et al.*, 2006a].

[14] CLM2.0 has one vegetation layer, a user defined number (by default 10) of soil layers, and up to 5 snow layers (depending on the snow depth). For this work, depths of the different soil nodes were set to 2.5, 5, 10, 20, 30, 50, 80, 120, 150 and 180 cm depth. Model parameters were obtained from a multiobjective calibration with inclusion of optimal initial state estimation for soil moisture in the OPE^3 field, as discussed by *De Lannoy et al.* [2006a]. The system for each profile was identified completely independent of all other profiles in the field. Deterministic simulations (no ensembles) with the calibrated model without filtering are referred to as the control model run.

[15] The model was run with a constant hourly time step and was set up for the distributed modeling of vertical soil moisture profiles at 36 points (grid cells, corresponding to the 36 working probes), with each grid cell containing 64 patches to represent the ensemble members.

3. Filtering Algorithm

3.1. State Estimation (ENKF)

[16] A state vector for 1 profile consists of 22 prognostic variables, i.e., canopy water storage, vegetation temperature, and soil temperature and moisture at 10 levels. Since the presence of snow was negligible and the soil temperature was only rarely below the freezing point during the studied period, state variables related to snow and frozen soil water were excluded. The state variables were taken at 36 points, resulting in a total state vector $\mathbf{x}_i$ of dimension $n = 22 \times 36 = 792$. However, the total state vector was subdivided into 22-element states for each individual profile to allow parallelized state updating (see below). The CLM2.0 represents the system that propagates the state in time (with discrete time steps i) and is denoted as $\mathbf{f}_{i,i-1}$, the discrete nonlinear transition function. The measurements, stored as an m-dimensional vector $\mathbf{y}_i$, are linked to the state by a discrete linear operator, the matrix $\mathbf{H}_i$, which contains only values of 0 and 1, because the observations used for assimilation were direct measurements of state variables, i.e., soil moisture. Depending on the number of observations assimilated at each time step i, the number of rows in $\mathbf{H}_i$ varied.

[17] The discrete nonlinear state-space representation of the system, i.e., the true process model, and the discrete linear transformation of the state to the observations, i.e., the measurement model, are given by

$$\mathbf{x}_i = \mathbf{f}_{i,i-1}(\mathbf{x}_{i-1}, \mathbf{u}_i, \mathbf{w}_{i-1}) + \mathbf{c}_i \tag{1}$$

$$\mathbf{y}_i = \mathbf{H}_i \mathbf{x}_i + \mathbf{v}_i \tag{2}$$

$\mathbf{u}_i$ is the vector of meteorological forcings $\mathbf{c}_i$ is a correction term (generally assumed to be zero) to account for possible systematic model error in $\mathbf{f}_{i,i-1}$, and $\mathbf{w}_i$ and $\mathbf{v}_i$ are random process and measurement noise, respectively. These random noise vectors are assumed white, zero mean Gaussian and independent. $\mathbf{Q}_i = \mathrm{E}[\mathbf{w}_i \mathbf{w}_i^T]$ and $\mathbf{R}_i = \mathrm{E}[\mathbf{v}_i \mathbf{v}_i^T]$ are positive definite covariance matrices describing the process and measurement noise.

[18] In absence of these sources of noise, the expression for the system is an ordinary differential equation and $\mathbf{x}_i$ would simply be its solution. In the presence of random noise $\mathbf{w}_i$, the probability density function (pdf) of $\mathbf{x}_i$ gives a complete statistical description of the state. An ensemble of forecasts ($j = 1, \cdots, N$) can be generated to obtain an estimate of the state's pdf and the best a priori estimate $\hat{\bar{\mathbf{x}}}_i^-$ of the state is given by

$$\hat{\mathbf{x}}_{j,i}^- = \mathbf{f}_{i,i-1}\left(\hat{\mathbf{x}}_{j,i-1}^+, \mathbf{u}_i, \mathbf{w}_{j,i-1}\right) \tag{3}$$

$$\hat{\bar{\mathbf{x}}}_i^- = \frac{1}{N}\sum_{j=1}^{N} \hat{\mathbf{x}}_{j,i}^- \tag{4}$$

with $\mathbf{w}_{j,i}$ a realization of the model error, which is imposed by perturbing forcings, parameters and/or states. The vector $\hat{\mathbf{x}}_{j,i-1}^+$ is an analysis that may be obtained from updating the state vector at time $i-1$ (see below), or, if no updating was performed at *i-1*, then formally $\hat{\mathbf{x}}_{j,i-1}^+ = \hat{\mathbf{x}}_{j,i-1}^-$. Note that the notation for the ensemble mean $\hat{\bar{\mathbf{x}}}_i^-$ (equation (4)) differs from that of ensemble members $\hat{\mathbf{x}}_{j,i}^-$ (equation (3)) only in the omission of the ensemble member subscript j. The $\sim$ is introduced here to indicate possible bias in the state estimate, which is not accounted for (bias-blind state estimate), while in the next section, a bias-corrected state will be estimated. The corresponding uncertainty is given by the a priori bias-blind state error covariance $\tilde{\mathbf{P}}_{x,i}^-$:

$$\tilde{\mathbf{P}}_{x,i}^- = \frac{1}{N-1}\left[\left[\hat{\mathbf{x}}_{1,i}^- \cdots \hat{\mathbf{x}}_{j,i}^- \cdots \hat{\mathbf{x}}_{N,i}^-\right] - \left[\hat{\bar{\mathbf{x}}}_i^- \cdots \hat{\bar{\mathbf{x}}}_i^- \cdots \hat{\bar{\mathbf{x}}}_i^-\right]\right] \cdot \left[\left[\hat{\mathbf{x}}_{1,i}^- \cdots \hat{\mathbf{x}}_{j,i}^- \cdots \hat{\mathbf{x}}_{N,i}^-\right] - \left[\hat{\bar{\mathbf{x}}}_i^- \cdots \hat{\bar{\mathbf{x}}}_i^- \cdots \hat{\bar{\mathbf{x}}}_i^-\right]\right]^T \tag{5}$$

which represents the spread in the a priori states as a result of perturbation of the initial states, parameters and forcings for the generation of ensemble members.

[19] Kalman filtering is used to correct the a priori state estimate (forecast) with observations. Each ensemble member j is updated individually, and the a posteriori state estimate (analysis) is obtained as follows:

$$\hat{\mathbf{x}}_{j,i}^+ = \hat{\mathbf{x}}_{j,i}^- + \tilde{\mathbf{K}}_{x,i}\left[\mathbf{y}_{j,i} - \mathbf{H}_i \hat{\mathbf{x}}_{j,i}^-\right] \tag{6}$$

$$\hat{\bar{\mathbf{x}}}_i^+ = \frac{1}{N}\sum_{j=1}^{N} \hat{\mathbf{x}}_{j,i}^+ \tag{7}$$

As discussed by *Burgers et al.* [1998], the observations $\mathbf{y}_i$ should be perturbed to assure sufficient spread, i.e. $\mathbf{y}_{j,i} = \mathbf{y}_j + \mathbf{v}_{j,i}$, with $\mathbf{v}_{j,i}$ the imposed perturbation. The optimal gain $\tilde{\mathbf{K}}_{x,i}$ is identical for all members and, as in the (extended) Kalman filter, given by *Kalman* [1960]:

$$\tilde{\mathbf{K}}_{x,i} = \tilde{\mathbf{P}}_{x,i}^- \mathbf{H}_i^T \left[\mathbf{H}_i \tilde{\mathbf{P}}_{x,i}^- \mathbf{H}_i^T + \mathbf{R}_i\right]^{-1} \tag{8}$$

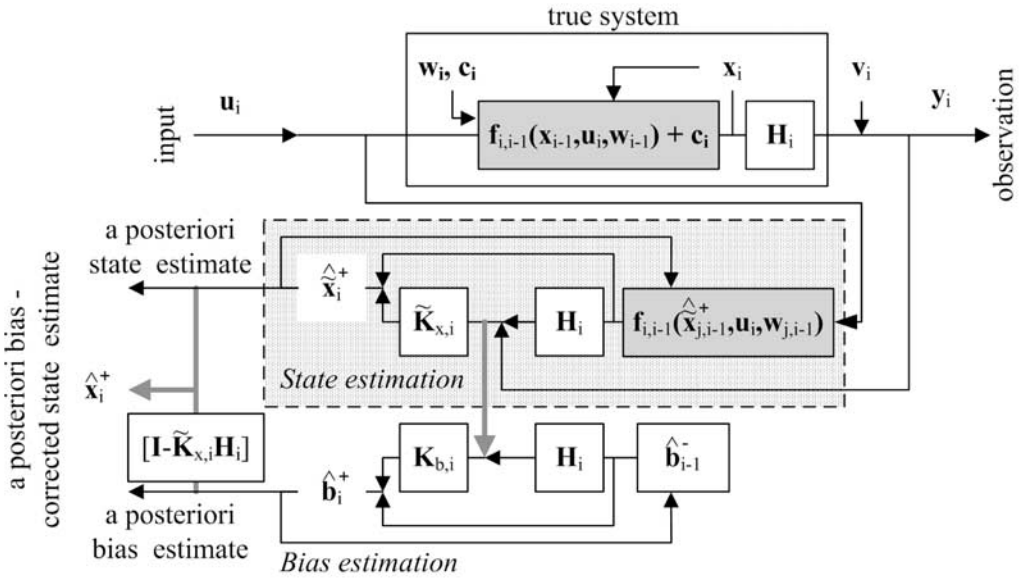

Figure 1. Two-stage state and bias estimation by two parallel Kalman filters. The solid gray box represents the (land surface) model. All symbols correspond to those in the text.

Analysis values obtained by equation (6) were constrained to avoid unrealistic analysis values. For example, soil moisture values above the effective porosity were set back to the value for the effective porosity.

3.2. Error Covariance Matrices for State Estimation: $\tilde{\mathbf{P}}_x^-$ and R

[20] To determine the ensemble error covariances in the $\tilde{\mathbf{P}}_x^-$ matrix, the information from 64 (N) member runs has been used, since for more members no significant improvement in the correspondence between the ensemble mean and the control model run was observed, and not much variability in higher-order ensemble moments was found with further increased ensemble sizes. The magnitude of the ensemble perturbation for all initial state variables, parameters and forcings was identical to that described by *De Lannoy et al.* [2006a]. A Gaussian perturbation was applied to parameters and initial states around the optimal mean found by calibration, and around the observed values for the forcings. For perturbed values exceeding some predefined limiting bounds, new values were drawn, because outlying members may have a strong impact on the empirical covariances.

[21] The individual grid cells were calibrated independently and the perturbation for one grid cell was chosen independent of that for another grid cell. The latter is a strong assumption with respect to the forcing errors, because for the studied 21 ha field the forcing errors are in reality almost perfectly correlated between (any two) different grid cells. For CLM2.0, which propagates information in the vertical direction only over the profile within the same grid cell, the a priori state error covariance matrix (found through the ensemble generation) should essentially be block diagonal with one block per grid cell: the perturbation for one patch in a grid cell does not affect any patch in another grid cell. All spurious elements off the diagonal blocks in the $\tilde{\mathbf{P}}_x^-$ matrix were very low and set to 0. This allowed for parallel state updating for the different individual profiles.

[22] The observation error covariance matrix **R** is determined by the uncertainty of the measurements. *Paltineanu and Starr* [1997] found root-mean-square error (RMSE) values of 0.009–0.030 cm^3/cm^3 for a nonlinear relationship between soil moisture content and the scaled frequency as obtained from capacitance probes. Therefore the uncertainty was chosen to be 0.0224 cm^3/cm^3, which is slightly lower than the upper RMSE value of 0.030 cm^3/cm^3. More specifically, **R** was set to 0.0005 **I**, with **I** the identity matrix, and assuming zero cross correlation between the observation errors. This uncertainty of 0.0224 cm^3/cm^3 ($\pm = \sqrt{0.0005}$) is less than the 0.05 cm^3/cm^3 upper limit that *Walker and Houser* [2004] found useful for data assimilation.

3.3. Bias Estimation (ENBKF)

[23] Optimal state estimation using a Kalman filter relies on the assumption of zero mean forecast error, i.e. $E[\mathbf{x}_i - \hat{\mathbf{x}}_i^-] = \mathbf{0}$, with $\hat{\mathbf{x}}_i^-$ a bias-free a priori state estimate. *De Lannoy et al.* [2006a] found that after calibration of the CLM2.0 for all individual profiles, the forecasted state estimates $\hat{\tilde{\mathbf{x}}}_i^-$ were biased in some soil layers, mainly for the deeper profiles. In addition, ensemble generation sometimes caused bias, so that $E[\mathbf{x}_i - \hat{\tilde{\mathbf{x}}}_i^-] = \mathbf{b}_i$. In case of bias, the state obtained by the procedure in the above section is a bias-blind analysis, which was denoted by $\hat{\tilde{\mathbf{x}}}_i^+$. In this study, the ENKF was extended with the bias estimation algorithm of *Friedland* [1969] to calculate the bias-corrected state estimate $\hat{\mathbf{x}}_i^+$. Figure 1 illustrates how a bias-blind state analysis $\hat{\tilde{\mathbf{x}}}_i^+$ and an a posteriori bias estimate $\hat{\mathbf{b}}_i^+$ are calculated separately by two Kalman filters and combined afterward.

[24] Within each grid cell, the bias-blind a priori and a posteriori state estimate are given by equation (4) and (7). The bias $\mathbf{b}_i$ consists of a vector of the same dimension as the state. For this study, it was propagated in time by a persistence model and it was not perturbed. The a posteriori

Table 1. Overview of DA Frequencies With Varying Numbers of Assimilation Events (N_{ass}) Over a Fixed Time Period, From 2 October 2001 through 19 March 2002

	Interval	N_{ass}
a	1 day	169
b	2 days	85
c	4 days	43
d	1 week	25
e	2 weeks	13
f	4 weeks	7
g	8 weeks	4

bias estimate, $\hat{\mathbf{b}}_i^+$, is found as a linear combination of the a priori bias estimate, $\hat{\mathbf{b}}_i^-$, and the difference between the observations and the a priori bias-corrected ensemble mean state estimate, $\hat{\mathbf{x}}_i^{-,-}$, as follows:

$$\hat{\mathbf{b}}_i^- = \hat{\mathbf{b}}_{i-1}^+ \tag{9}$$

$$\hat{\mathbf{x}}_i^{-,-} = \hat{\tilde{\mathbf{x}}}_i^- + \hat{\mathbf{b}}_i^- \tag{10}$$

$$\hat{\mathbf{b}}_i^+ = \hat{\mathbf{b}}_i^- + \mathbf{K}_{b,i}\left[\left(\mathbf{y}_i - \mathbf{H}_i\hat{\tilde{\mathbf{x}}}_i^-\right) - \mathbf{H}_i\hat{\mathbf{b}}_i^-\right] \tag{11}$$

$$= \hat{\mathbf{b}}_i^- + \mathbf{K}_{b,i}[\mathbf{y}_i - \mathbf{H}_i\hat{\mathbf{x}}_i^{-,-}] \tag{12}$$

[25] The double superscript $-,-$ is used for an a priori state estimate which is corrected by an a priori bias estimate. The weighting factor $\mathbf{K}_{b,i}$ is defined by [*Friedland*, 1969; *Dee and da Silva*, 1998]

$$\mathbf{K}_{b,i} = \mathbf{P}_{b,i}^-\mathbf{H}_i^T\left[\mathbf{H}_i\mathbf{P}_{b,i}^-\mathbf{H}_i^T + \mathbf{H}_i\tilde{\mathbf{P}}_{x,i}^-\mathbf{H}_i^T + \mathbf{R}_i\right]^{-1} \tag{13}$$

with $\mathbf{P}_{b,i}^-$ the a priori bias error covariance, which was derived empirically (see below). The resulting bias-corrected a posteriori state estimate $\hat{\mathbf{x}}_i^+$ is given by [*Friedland*, 1969; *Dee and da Silva*, 1998]

$$\hat{\mathbf{x}}_{j,i}^+ = \hat{\tilde{\mathbf{x}}}_{j,i}^+ + \left[\mathbf{I} - \tilde{\mathbf{K}}_{x,i}\mathbf{H}_i\right]\hat{\mathbf{b}}_i^+ \tag{14}$$

[26] The state error covariance for bias-corrected a posteriori state estimates is $\mathbf{P}_{x,i}^+ = \tilde{\mathbf{P}}_{x,i}^+ + [\mathbf{I} - \tilde{\mathbf{K}}_{x,i}\mathbf{H}_i]\mathbf{P}_{b,i}^+[\mathbf{I} - \tilde{\mathbf{K}}_{x,i}\mathbf{H}_i]^T$. The bias-corrected state estimate is a more precise estimate than the a posteriori bias-blind state, i.e., its (ensemble) mean value is closer to the truth. However, since the bias-blind state is corrected by another random variable, the bias estimate, the uncertainty for the bias-corrected a posteriori state estimate is larger, or the accuracy is lower.

3.4. Error Covariances and Gain Factor for Bias Estimation: $\mathbf{P}_b^-$ and $\mathbf{K}_b$

[27] If the bias-blind a priori state error covariance $\tilde{\mathbf{P}}_{x,i}^-$ is available as the result of an effort to properly estimate it, as is the case for an ENKF in this study, then the matrix $\mathbf{P}_{b,i}^-$ can be approximated as fraction of $\tilde{\mathbf{P}}_{x,i}^-$ [*Dee and da Silva*, 1998]:

$$\mathbf{P}_{b,i}^- = \frac{\gamma}{1-\gamma}\tilde{\mathbf{P}}_{x,i}^- \tag{15}$$

such that the gain for the bias estimation can be found as

$$\mathbf{K}_{b,i} = \gamma\tilde{\mathbf{P}}_{x,i}^-\mathbf{H}_i^T\left[\mathbf{H}_i\tilde{\mathbf{P}}_{x,i}^-\mathbf{H}_i^T + (1-\gamma)\mathbf{R}_i\right]^{-1} \tag{16}$$

In this formula for $\mathbf{K}_{b,i}$, γ can take any positive value, depending on the dynamics of the system and it is not necessarily restricted to $0 \leq \gamma < 1$ as in equation (15). This parameter could be tuned to optimize the filtering system [*Keppenne et al.*, 2005]. The larger γ, the more the a priori bias estimate is updated by observational information. However, for $\gamma \geq 1$, the tuning of $\mathbf{K}_{b,i}$ is entirely empirical, and because equation (15) is not valid anymore, it becomes unclear how to assess $\mathbf{P}_{b,i}^-$. In this study, scenarios with $\gamma = 0.5$ were tested, without any effort for optimization.

4. Scenario Analysis

[28] CLM2.0 was set up for distributed soil moisture modeling over 36 profiles (grid cells), but because of our assumption that observation and model (including forcing) errors were uncorrelated for any two grid cells, the model run (and assimilation) for each grid cell was completely independent of the other grid cells and can be considered as individual profile simulation. For all profiles, assimilation of soil moisture observations at varying depths (DA depths = data assimilation depths) and for varying frequencies (DA frequencies = data assimilation frequencies) was performed. Depending on the case study, only assimilation into 1 soil layer was performed or in all soil layers where observations were available. The assimilation events were chosen within a fixed time period from 2 October 2001 through 19 March 2002 with seven different DA frequencies as summarized in Table 1.

[29] To quantify the assimilation effect, the RMSE for an individual layer (l), was determined by $\sqrt{\frac{1}{T_l}\sum_{i=1}^{T_l}(\hat{\tilde{x}}_i - y_i)_l^2}$, with $\hat{\tilde{x}}_i$ and y_i respectively the scalar ensemble mean model output and the observation at the time instant i of soil moisture in layer l. T_l is the number of time steps for which data are available in layer l during the validation period (2 October 2001 through 30 April 2002). For ENBKF, $\hat{\tilde{x}}_i$ is replaced by $\hat{x}_i$. The profile-integrated RMSE was calculated by $\sqrt{\frac{1}{\sum_{l=1}^{L}T_l}\sum_{l=1}^{L}\sum_{i=1}^{T_l}\left(\hat{\tilde{x}}_i - y_i\right)_l^2}$, with L the number observation of layers for a probe. No weights for layer depths were included, resulting in relatively more weight to the (thinner) surface layers.

4.1. Case Study 1 (ENKF)

4.1.1. Assimilation in One Layer

[30] In a first experiment, the state of the soil moisture profile was estimated by filtering observations in a single soil layer, without bias correction. The ENKF columns in Table 2 and Figure 2 show complementary information to assess the impact of the DA depth on the soil moisture profile estimate obtained by the ENKF. Table 2 shows, for 24 B and D probes, the RMSE values integrated over the complete profiles for the control run and the ensemble mean run without filtering, and differences in profile-integrated RMSE for the ENKF runs with the ensemble mean without filtering for all 7 DA depths, for an 8-weekly assimilation interval. As discussed by *De Lannoy et al.* [2006a], for

Table 2. Profile-Integrated RMSE for the Control and Ensemble Mean Run Without Filtering for Selected Probes and Differences (ENKF - Ens Mean) and (ENBKF - Ens Mean) in Profile-Integrated RMSE for ENKF and ENBKF for 8-weekly Assimilation in Different Individual DA Depths[a]

			DA Depth, cm													
			ENKF							ENBKF						
Probe	Control	Ens Mean	10	30	50	80	120	150	180	10	30	50	80	120	150	180
BH1	2.91	2.35	0.00	−0.13	—	−0.17	—	—	—	0.04	−0.53	—	−0.29	—	—	—
BH2	2.91	2.32	−0.03	0.03	—	0.03	—	—	—	0.62	−0.03	—	0.02	—	—	—
BH3	2.16	2.70	−0.02	0.01	—	0.00	—	—	—	−0.32	−0.18	—	0.01	—	—	—
BH4	3.21	6.92	−1.43	−0.31	—	−2.26	—	—	—	−3.73	−0.60	—	−2.73	—	—	—
BL1	9.03	9.15	0.38	−0.22	−0.32	−0.06	0.05	0.15	0.82	0.84	−0.61	−0.78	−0.16	0.04	−1008.15	2.27
BL2	8.81	9.11	−0.23	−0.03	0.20	−0.70	−0.13	−1.91	−1.08	−0.35	−0.04	0.33	−1.00	−0.19	−1.71	−0.90
BL3	6.60	6.36	0.02	0.13	0.06	0.00	0.07	0.42	0.29	0.03	0.19	0.07	0.02	0.06	0.44	1.02
BL4	6.06	5.92	0.00	−0.01	−0.18	−0.04	−0.83	−0.36	−0.65	0.11	0.00	−0.28	−0.51	−2.88	−0.79	−1.51
BM1	4.46	4.57	−0.02	−0.01	−0.08	—	−0.02	0.08	−0.50	0.27	−0.17	−0.17	—	0.00	0.09	−0.81
BM2	9.01	10.97	−0.10	0.01	−0.55	—	0.16	−0.40	−0.21	−0.72	−0.07	−1.05	—	0.00	−0.74	−5.11
BM3	4.75	4.24	−0.11	−0.02	−0.06	—	0.04	−0.34	−0.64	−0.05	−0.02	−0.10	—	0.04	−0.58	−1.03
BM4	6.55	7.20	0.01	−0.94	−1.02	—	−0.57	−1.01	−1.85	0.02	−1.34	−1.40	—	−0.55	−1.28	−2.91
DH1	2.41	3.14	−0.19	0.07	—	−0.44	—	—	—	−0.18	0.08	—	−1.40	—	—	—
DH2	2.42	2.74	−0.20	−0.04	—	−0.19	—	—	—	−0.46	−0.17	—	−0.28	—	—	—
DH3	2.62	6.30	−0.55	−0.54	—	−0.37	—	—	—	−3.18	−1.84	—	−1.07	—	—	—
DH4	4.36	4.07	−0.10	−0.41	—	0.07	—	—	—	−0.34	−1.65	—	0.15	—	—	—
DL1	2.86	5.05	−0.46	−0.88	−0.99	−0.41	−0.18	0.05	−0.64	−1.14	−2.01	−2.56	−0.77	−0.24	0.11	−1.20
DL2	5.16	5.95	−0.15	−0.04	−0.02	−0.34	−0.03	0.16	−0.11	−0.60	−0.07	−0.05	−2.43	0.01	0.23	−0.23
DL3	9.86	10.83	−0.05	0.33	0.55	−1.53	−0.70	−1.48	−0.90	−0.26	0.24	0.59	−2.54	−0.75	−3.41	−1.43
DL4	9.29	11.64	−0.17	−0.31	−1.30	−1.00	−1.78	−1.33	−1.73	−0.17	−0.50	−2.07	−1.58	−5.14	−2.25	−3.09
DM1	3.84	9.14	−0.06	−0.59	−1.54	—	−3.06	−0.60	−0.29	−0.15	−0.92	−2.15	—	−4.22	−0.97	−0.51
DM2	5.25	6.34	0.31	−0.14	−0.41	—	−0.04	0.03	0.04	−0.66	−0.07	0.09	—	−0.09	−0.04	0.00
DM3	5.19	6.07	−0.05	0.02	0.37	—	−0.40	−0.30	−0.24	−0.08	0.03	−0.04	—	−0.79	−0.37	−0.44
DM4	8.28	9.53	0.09	−0.35	−0.47	—	−0.56	−0.63	−0.58	0.16	−0.46	−1.01	—	−0.60	−0.88	−2.94

[a]Values are in vol%. Control indicates the control run; Ens Mean indicates ensemble mean without filtering. Dashes indicate no possibility for assimilation at the given depth.

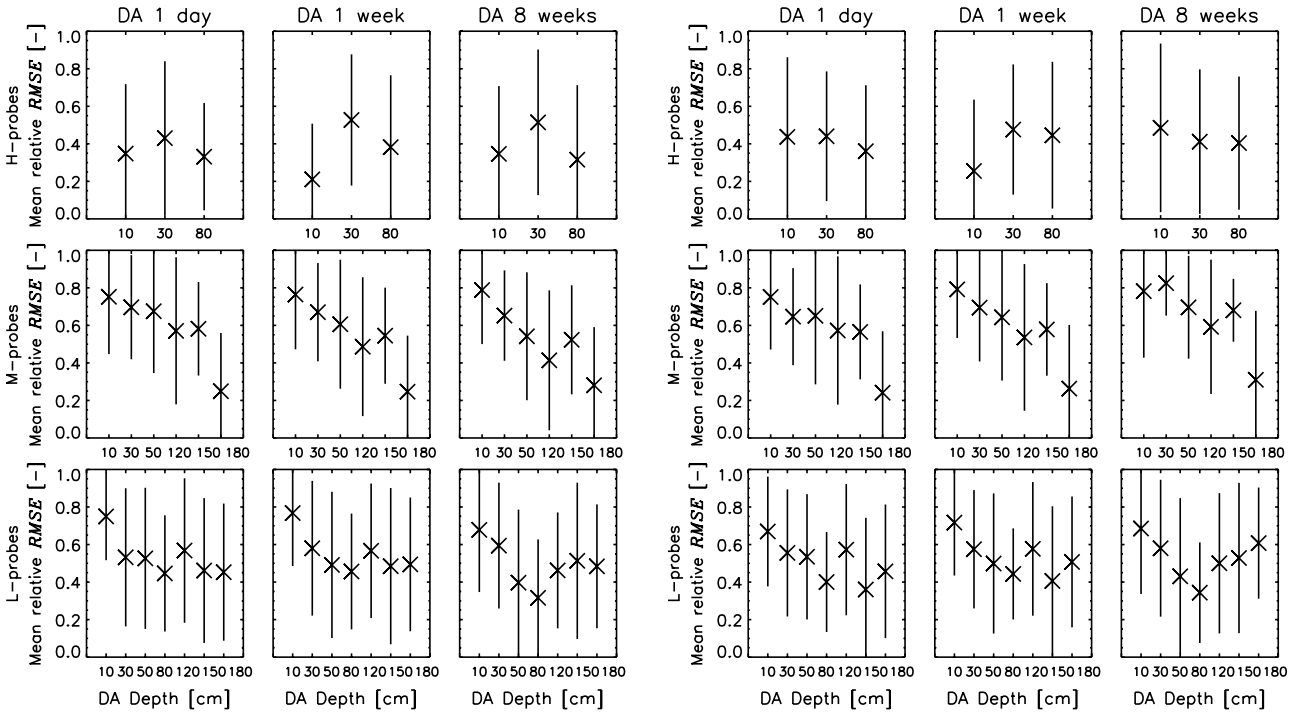

Figure 2. Mean relative values for the profile-integrated RMSE as function of the DA depth for 3 different DA frequencies (variable amount of observations) and per probe type for (left) ENKF and (right) ENBKF.

some probes a lower performance was found for the ensemble mean without filtering than for the control run. This is also why the performance after filtering was sometimes less than the control run. However, for most probes the RMSE for the ENKF run was lower than for the ensemble mean without filtering.

[31] The influence of the DA depth on the profile-integrated RMSE is summarized in Figures 2 for 3 different DA frequencies (the results for an 8-weekly DA frequency contain those in Table 2). For assimilation at each individual DA depth, the profile-integrated RMSE for each of the 36 single profiles was determined. Per profile, the lowest RMSE, i.e., $RMSE_{\min}$ found for assimilation at the most successful DA depth and the highest profile-integrated RMSE, i.e. $RMSE_{\max}$ were sought. The profile-integrated RMSE obtained by assimilation at each DA depth was linearly rescaled by $\frac{\mathrm{RMSE}-RMSE_{\min}}{RMSE_{\max}-RMSE_{\min}}$. The (spatial) average and standard deviation of the rescaled RMSE values over all profiles were then plotted as function of the DA depth. This rescaling was performed to understand the relative impact of filtering at different DA depths per probe, without comparison to any reference run and to weight the contribution of each profile equally in the spatial mean.

[32] Figure 2 then shows that it was best to assimilate soil moisture at 80 cm depth to improve the complete soil moisture profile estimate for L probes and at 180 cm for M probes. For H probes, it was not clear for which DA depth the RMSE was lowest. Assimilation at 10 cm, which is closest to a surrogate for remote sensing data, was generally not a good option to obtain an overall improvement over a deep profile (M and L probes), because the corresponding improvement for the deeper layers was only limited. This might be due to a decoupling of the topsoil layers from the deeper layers and to the very complex geohydrology observed in the deeper soil layers of the OPE^3 field. To estimate shallow profiles (H probes), top layer (10 cm) soil moisture assimilation was more useful. The spread on the mean relative RMSE values was quite large, and therefore it is difficult to accept these general findings for individual profiles. Also, these results are function of the calibration. For some layers the model corresponded very well to the observations and assimilation had almost no effect, such as for the H probes, where the calibration was very successful in all 3 observed soil layers and the choice of the DA depth was of limited importance. On the other hand, assimilation in biased layers caused a reduction of bias in that layer and a general improvement in the profile-integrated measure. *Dee and da Silva* [1998] have shown that in the presence of bias, the Kalman filter for state estimation only is able to correct for this bias in a suboptimal way. This is also the idea behind the practice of covariance inflation to deal with model bias in a conventional Kalman filter.

[33] However, the profile-integrated RMSE might suggest an improvement, while this is not necessarily true for all individual layers. For example, in Figure 3 assimilation at 80 cm depth for probe DL3 (for which the calibration did not yield good results for all layers) decreased the performance in the 3 layers above 80 cm, while the profile-integrated RMSE was improved (see Table 2, where RMSE for filtering at 80 cm - RMSE for the ensemble mean without filtering = -1.54 vol%). Because of the presence of bias in the innovations for the assimilation layer, the performance for neighboring soil layers may degrade, rather than improve, even if $\tilde{\mathbf{P}}_x^-$ would be exact. Because forecast bias was observed in all profiles which were calibrated for more than 3 soil layers of observations, there is a need for bias removal during assimilation. For some profiles the approximate estimation of $\tilde{\mathbf{P}}_{x,i}^-$ by the ensemble perturbation (only 64 members) also resulted in an inaccurate propagation of the innovations to other layers.

[34] Despite of the clear presence of bias and the suboptimality of the filter, the ENKF columns in Table 3 show that even for a few assimilation events in a single soil layer, the root spatial (over all profiles in the OPE^3 field) mean squared error for each soil layer individually was always slightly reduced compared to the ensemble mean without filtering, independent of the chosen DA depth.

[35] Comparison of the absolute values of the profile-integrated RMSE revealed that the DA frequency had less influence on the performance than the choice of the DA depth. Figure 4 shows for each DA depth the spatial means and standard deviations of relative profile-integrated RMSE values (averaged over all probes with observations available at the single considered DA depth) as function of the DA frequency. The rescaling of the RMSE was similar to that in Figure 2, but it is now for comparing experiments with different DA frequencies at each single DA depth. The number of probes contributing to the mean values is dependent on the DA depth: for assimilation at 10 and 30 cm depth, all 36 active probes contribute, for assimilation at 50, 120, 150 and 180 cm depth, only 24 M and L probes participate and for assimilation at 80 cm, only 24 H and L probes are taken into account. For most DA depths, the optimal DA frequency with the ENKF (Figure 4, top) was once a week or every 2 weeks. More frequent assimilation was only beneficial to the profile estimate for assimilation at 80 cm and 180 cm, which are exactly the layers where assimilation most improved the profile-integrated RMSE for the deeper profiles. The decreased performance for more frequent assimilation at other DA depths is entirely due to erroneous propagation of the (sometimes biased) innovations over the profile layers outside the assimilation layer. The RMSE in a single layer always decreased for more intensive assimilation in that particular layer (not shown).

[36] In a separate experiment, it was found that assimilation in a single layer at the beginning of the validation period only could not guarantee a good evolution of the complete state, because the update was not propagated well to all layers (causing model shocks) and because of model errors. Therefore repeated assimilation was needed to enhance the time mean state estimate.

4.1.2. Assimilation in All Soil Layers

[37] In a second experiment, the assimilation of all available observations for a profile at each assimilation time was studied, to evaluate the effect of varying DA frequencies. Table 4 shows a considerable improvement in the profile-integrated RMSE over the ensemble mean without filtering at any DA frequency.

[38] In Figure 5, the effect on the individual soil layers is studied as a result of complete profile assimilation. For each single layer, the difference in RMSE between the filter run and the ensemble mean without filtering was calculated.

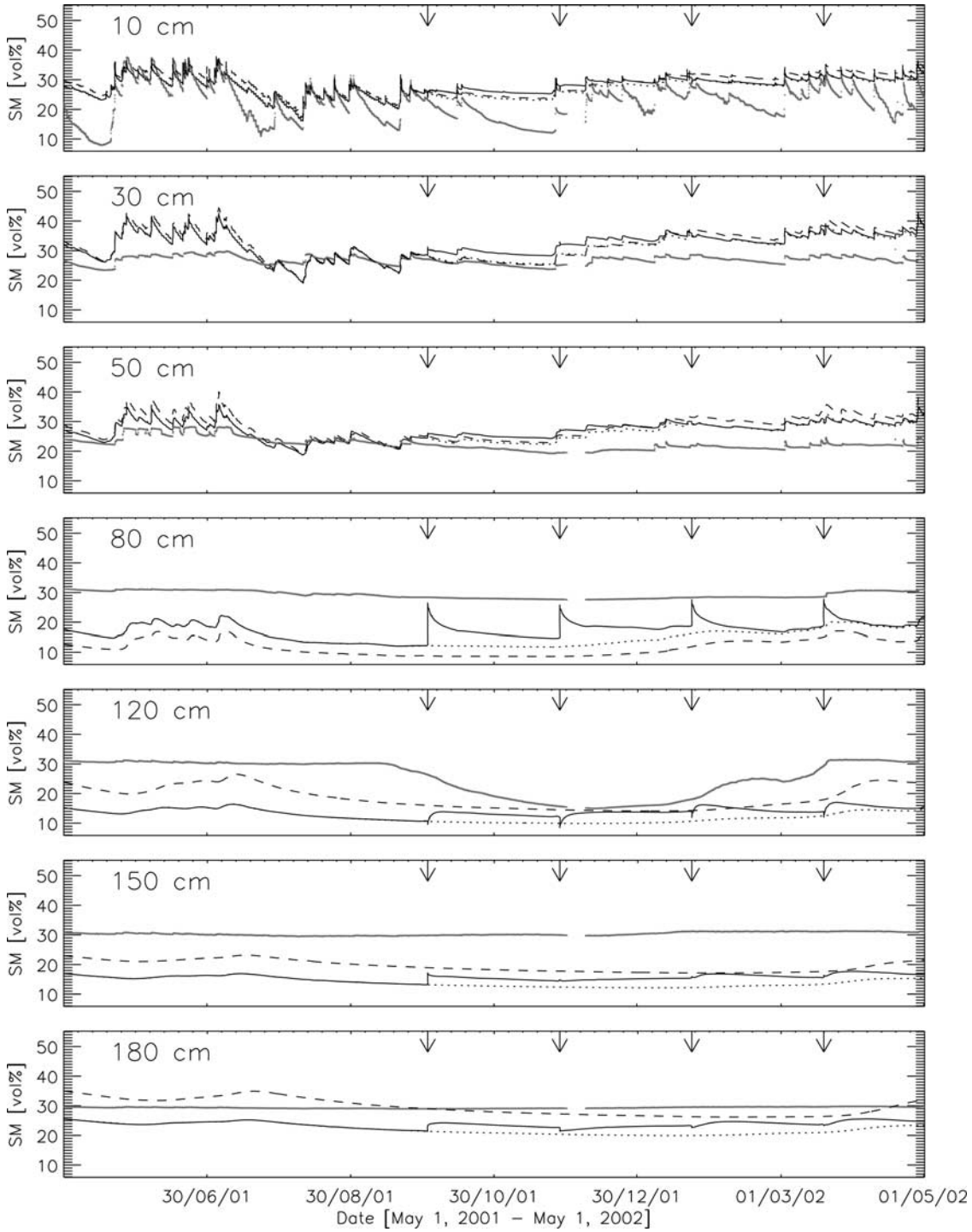

Figure 3. Soil moisture (SM) time series at DL3 with observations (shaded), the control run (dashed line), the ensemble mean run without filtering (dotted line), and the ENKF run (solid line) with 8-weekly assimilation at 80 cm. The arrows indicate the filtering time steps.

Table 3. Root Spatial Mean Square Error for the Control and Ensemble Mean Run Without Filtering at Individual Soil Layers and Differences in RMSE (ENKF - Ens Mean) and (ENBKF - Ens Mean) for 8-weekly Assimilation at Different DA Depths[a]

			DA Depth, cm													
			ENKF							ENBKF						
Layer, cm	Control	Ens Mean	10	30	50	80	120	150	180	10	30	50	80	120	150	180
10	2.00	2.15	−0.07	0.00	0.00	−0.04	0.01	−0.01	0.00	−0.60	−0.02	0.00	−0.09	0.04	−0.04	−0.04
30	1.87	2.00	−0.03	−0.17	−0.11	−0.07	−0.02	−0.02	0.00	0.02	−0.84	−0.10	−0.09	0.01	0.00	0.03
50	2.58	2.82	0.00	−0.10	−0.28	−0.05	−0.05	−0.04	0.02	0.02	−0.14	−1.41	−0.09	−0.01	−0.06	−0.01
80	2.12	2.21	−0.11	−0.06	−0.09	−0.30	−0.05	−0.08	−0.03	−0.16	−0.12	−0.16	−1.11	−0.07	−0.16	0.00
120	2.23	2.53	0.01	−0.05	−0.04	−0.06	−0.26	−0.04	−0.07	0.07	−0.09	−0.04	−0.06	−1.23	−0.01	−0.03
150	2.28	2.55	0.00	−0.05	−0.05	−0.06	−0.16	−0.29	−0.04	−0.02	−0.07	−0.06	−0.08	−0.09	−0.98	−0.07
180	2.80	3.23	−0.04	−0.03	−0.04	−0.07	−0.14	−0.12	−0.38	−0.08	−0.05	−0.05	−0.08	−0.17	−0.23	−1.61

[a]Values are in vol%. Control indicates the control run; Ens Mean indicates ensemble mean without filtering.

These differences in performances were linearly scaled between 0 and 1 and, per depth, were spatially averaged over all probes of the same type. The mean relative differences in RMSE indicated that profile assimilation had most effect on the deeper layers. The upper layers, and especially the layer at 10 cm, were only slightly improved by profile assimilation. This may be due to three reasons. First, more bias was in general found for deeper layers after calibration, causing a larger assimilation correction than in the less biased upper layers. Second, the finer discretization in the upper part of the profile leads to some layers that do not have a corresponding observation. For these layers updates are performed via correction propagation (by $\tilde{\mathbf{P}}_x^-$), which might not always be correct and may counteract the updates in the surrounding layers. Another reason is that corrections in the topsoil layers persist for shorter periods, due to a larger influence of the atmospheric forcings.

[39] Figure 6 (left) shows that more frequent assimilation events of complete profiles always improves the soil moisture profile estimate during the validation period.

4.2. Case Study 2 (ENBKF)

[40] Since the assimilation experiments in the previous section clearly showed problems due to the presence of bias, combined state and bias estimation was studied. A persistence bias model was considered ($\hat{\mathbf{b}}_i^- = \hat{\mathbf{b}}_{i-1}^+$, with $\hat{\mathbf{b}}_0 = \mathbf{0}$) and $\gamma = 0.5$ was tested.

4.2.1. Assimilation in One Layer

[41] The ENBKF columns in Table 2 give the differences between profile-integrated RMSE for all probes for ENBKF assimilation every 8 weeks at the 7 different DA depths and the ensemble mean without filtering. Overall, for all DA depths the complete state estimate was enhanced compared to the results for bias-blind state estimation only. The measures varied with DA depth similarly to what was found for state estimation only (Figure 2, right).

[42] Closer investigation of the performance for the individual layers in Table 5 for assimilation once a week revealed that the improvement over the complete profile was mostly due to an improvement for the assimilation layer. The fact that layers surrounding the assimilation layer did not always benefit from the bias correction suggests problems for the practical implementation. A first problem is the assumed bias model and the initialization of the bias. The bias in all profile layers cannot be retrieved through assimilation in a single layer, because there is no knowledge on the vertical variability of the bias included in the bias model: the bias system is not observable, if observations are

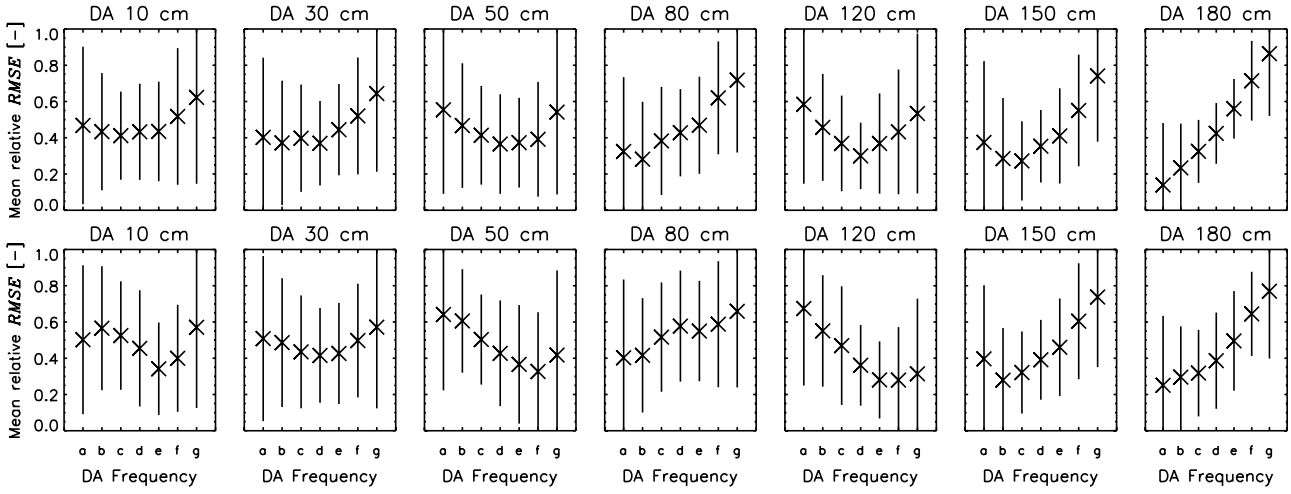

Figure 4. Influence of DA frequency on the mean relative values for the profile-integrated RMSE for (top) ENKF and (bottom) ENBKF at each DA depth.

Table 4. Differences in Profile-Integrated RMSE (ENKF-Ensemble Mean Without Filtering) and (ENBKF - Ensemble Mean Without Filtering) for Assimilation of All Available Observations in a Profile at a Weekly and 8-weekly DA Frequency[a]

	DA Frequency			
	ENKF		ENBKF	
Probe	d	g	d	g
BH1	−0.49	−0.23	−1.15	−0.64
BH2	0.03	0.00	−0.41	0.04
BH3	−0.16	−0.02	−1.57	−0.82
BH4	−2.61	−2.24	−5.04	−4.19
BL1	−2.66	−0.96	−5.05	−3.35
BL2	−4.61	−2.56	−5.83	−3.53
BL3	−0.89	−0.17	−3.78	−2.52
BL4	−1.70	−0.94	−4.48	−3.84
BM1	−1.42	−0.60	−3.39	−2.81
BM2	−1.71	−0.69	−9.27	−7.15
BM3	−1.48	−0.63	−2.92	−2.22
BM4	−3.17	−2.32	−5.39	−4.62
DH1	−0.91	−0.50	−2.06	−1.47
DH2	−0.37	−0.26	−1.34	−0.98
DH3	−1.83	−0.72	−4.72	−4.16
DH4	−1.39	−0.39	−2.73	−1.72
DL1	−1.80	−1.29	−3.64	−3.19
DL2	−1.33	−0.50	−4.45	−3.69
DL3	−4.28	−2.36	−8.28	−7.41
DL4	−2.91	−1.94	−9.24	−7.80
DM1	−4.14	−2.95	−7.49	−6.61
DM2	−1.75	−0.80	−4.82	−4.54
DM3	−1.96	−0.79	−4.71	−4.16
DM4	−3.03	−1.76	−7.99	−6.85

[a]Values are in vol%.

not available for all layers. The constant bias model is basically an identity matrix $\mathbf{I}$, so that the rank of the observability matrix [*Maybeck*, 1979] for the bias system never can reach n if not all n bias variables corresponding to the n state variables are measured somehow. A second problem is the estimation of the state error covariance $\tilde{\mathbf{P}}^{-}_{x,i}$ and the assumption that $\mathbf{P}^{-}_{b,i}$ would be proportional to $\tilde{\mathbf{P}}^{-}_{x,i}$. On the basis of this assumption, it is normal that improper propagation of random error corrections (for a regular Kalman filter without bias removal) also introduces inaccurate propagation of bias corrections over the profile. Further, for this study, there was no physical evidence that $\mathbf{P}^{-}_{b,i}$ would be proportional to $\tilde{\mathbf{P}}^{-}_{x,i}$ and more accurate covariance models would definitely further enhance the filter's performance.

[43] The ENBKF columns in Table 3 show that for assimilation in a single soil layer, the root spatial (over all probes in the OPE^3 field) mean squared error was generally reduced at the chosen DA depth compared to the ensemble mean without filtering, while the other layers were only marginally affected.

[44] Also in the assimilation layer, the results could be further improved, e.g., by the use of a different bias model other than a persistence model. Figure 7 shows the temporal evolution of soil moisture at 80 cm for the DL3 probe, which shows bias in this layer, with assimilation every 8 weeks. Figure 8 shows the complete profile around the first assimilation event. The zoom plot in Figure 7 displays how the analysis almost equals the observations at the assimilation time step. After assimilation, the influence of the bias-blind state update (containing a bias part) is still

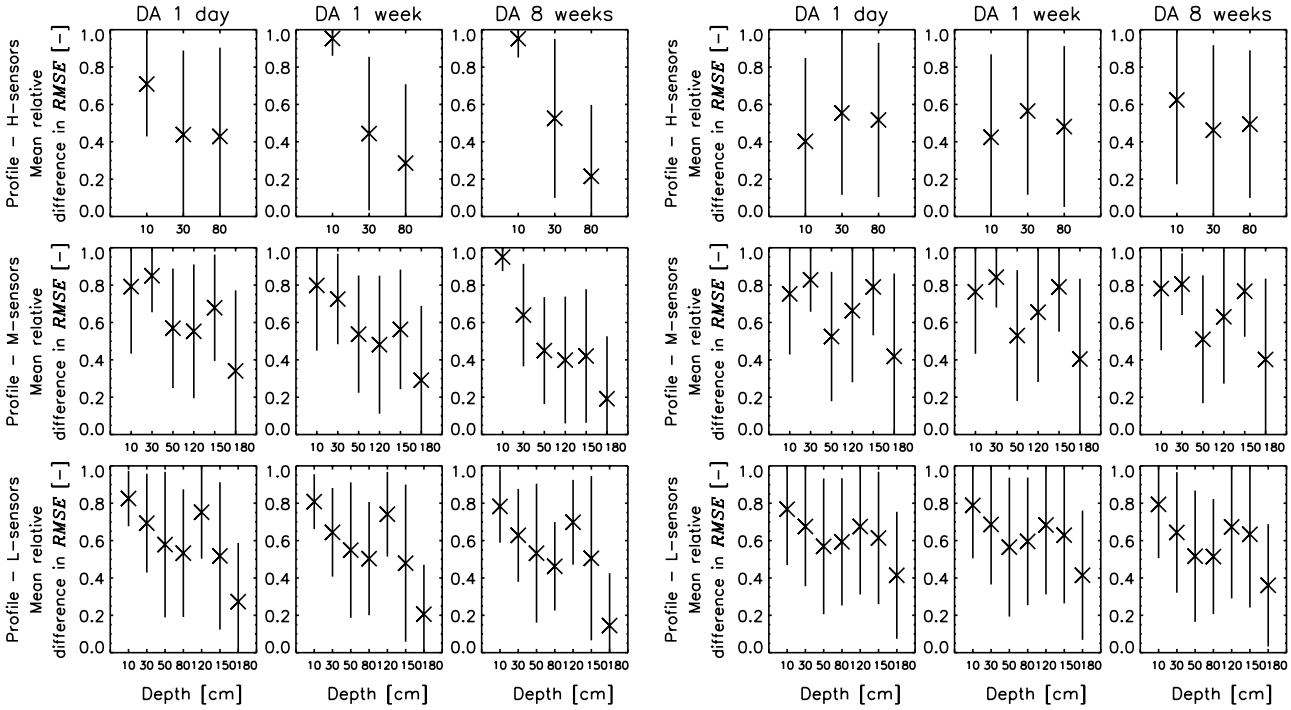

Figure 5. Means of relative differences (filter run-ensemble mean without filtering) in RMSE for the individual soil layers for assimilation ((left) ENKF and (right) ENBKF)) of all available observations in the profiles.

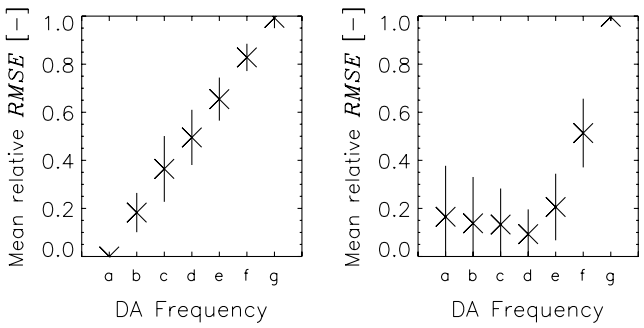

Figure 6. Mean relative profile-integrated RMSE for profile assimilation with (left) ENKF and (right) ENBKF as a function of varying numbers of observations in time.

persisting and slowly disappears, which causes an overshoot in the predicted bias-corrected state estimate due to an additional bias term in $\hat{\mathbf{x}}_i^- = \hat{\hat{\mathbf{x}}}_i^- + \hat{\mathbf{b}}_{i-1}^+$, as long as the influence of the bias-blind state update is present. This problem is further discussed in a subsequent paper (De Lannoy et al., submitted manuscript, 2006).

[45] Figure 4 (bottom) shows that the effect of the DA frequency on the profile-integrated RMSE for ENBKF depended on the DA depth in a similar way as for ENKF. However, for ENKF the soil moisture estimate in the individual soil layers always improved with more intensive assimilations, while for ENBKF the optimal DA frequency was about 2 weeks (almost independent of the DA depth) and more intense assimilation generally did not further improve the results (not shown).

4.2.2. Assimilation in All Soil Layers

[46] Through assimilation of all available observations in a profile, less negative effects from incorrectly initialized bias and erroneous vertical correction propagation can be expected (Table 4). Again for the upper layers, there was least advantage from profile assimilations, except for H probes (Figure 5).

[47] Figure 9 shows the root of the spatial (over all probes) mean square error for some individual layers, in the case of 4 assimilation events of all available profile information in the field. It is clear that after assimilation, the error in all layers is reduced far below the value for the control run.

[48] To obtain the best results with ENBKF, it is advised to assimilate at a DA frequency of 1 or 2 weeks (Figure 6). In contrast to the ENKF, more intensive assimilations did not further improve the overall profile or individual layer results. A DA frequency of 1 or 2 weeks is slightly less than the temporal autocorrelation length found for soil moisture in the top layer of the OPE[3] field [*De Lannoy et al.*, 2006b]. This autocorrelation length for soil moisture depends on the atmospheric forcings. While for meteorological applications, the optimal DA frequency was found to depend on the model [*McPherson*, 1975], for bounded hydrological problems, like the estimation of soil moisture, the forcings (mainly precipitation) will have a large impact.

5. Filter Performance

5.1. Normalized Profile-Integrated RMSE

[49] Figure 10 shows spatial means of normalized profile-integrated RMSE values for different probe types as function of the kind of model run. For each probe, the RMSE values resulting from the different experiments were divided by the RMSE obtained for the ensemble mean run without filtering for that probe, to evaluate the different experiments with respect to this reference run. A spatial average of the resulting normalized RMSE values over all probes of the same type was calculated. Here, no linear rescaling of the profile-integrated RMSE for the different experiments was performed, as was the case for the "relative" RMSE in

Table 5. RMSE for the Ensemble Mean Without Filtering (Ens Mean) In Each Individual Profile Layer and Difference in RMSE (ENBKF - Ens Mean) for Weekly Assimilation at 80 cm[a]

	Ens Mean							ENBKF						
Layer, cm	10	30	50	80	120	150	180	10	30	50	80	120	150	180
BH1	2.28	2.78	—	1.91	—	—	—	0.10	−0.36	—	−1.11	—	—	—
BH2	3.60	1.40	—	1.11	—	—	—	0.31	0.19	—	−0.55	—	—	—
BH3	4.06	2.05	—	1.07	—	—	—	−0.01	0.23	—	−0.68	—	—	—
BH4	9.07	3.35	—	7.09	—	—	—	−2.40	−1.59	—	−6.39	—	—	—
BL1	3.19	7.17	7.57	1.86	2.32	13.54	16.58	0.35	−0.33	−0.84	−1.01	−0.19	−0.38	0.36
BL2	5.37	1.66	1.83	5.25	2.24	17.06	14.89	−2.11	0.21	2.23	−3.53	−0.23	−1.57	−1.04
BL3	9.51	4.79	4.82	1.24	1.27	6.78	9.88	−0.73	1.07	0.77	−0.75	0.16	1.52	−1.39
BL4	2.68	1.05	3.80	6.12	10.21	4.25	7.95	−0.13	0.72	1.48	−5.00	−1.20	−0.77	0.04
DH1	2.63	0.74	—	4.70	—	—	—	0.05	0.01	—	−4.11	—	—	—
DH2	3.78	1.75	—	2.29	—	—	—	−0.12	0.31	—	−1.67	—	—	—
DH3	8.48	5.75	—	3.77	—	—	—	−1.13	−0.92	—	−2.98	—	—	—
DH4	3.96	5.41	—	2.15	—	—	—	0.32	0.35	—	−1.52	—	—	—
DL1	3.82	7.37	9.21	1.98	2.09	1.65	3.71	−0.55	−1.44	−1.75	−1.18	−0.30	0.78	−0.93
DL2	4.92	1.73	1.39	13.64	0.82	2.70	4.94	−2.02	−0.81	0.03	−11.57	1.55	2.19	3.21
DL3	6.64	5.98	6.19	13.43	11.77	17.60	8.59	0.37	2.64	1.76	−10.68	−0.35	−3.20	0.04
DL4	4.24	2.59	8.50	4.87	23.49	8.41	14.33	−0.40	−1.40	−2.18	−4.02	−1.65	−4.80	−2.88

[a]Values are in vol%. For M probes, no observations at 80 cm are available for assimilation. Dashes appear where no validation data are available.

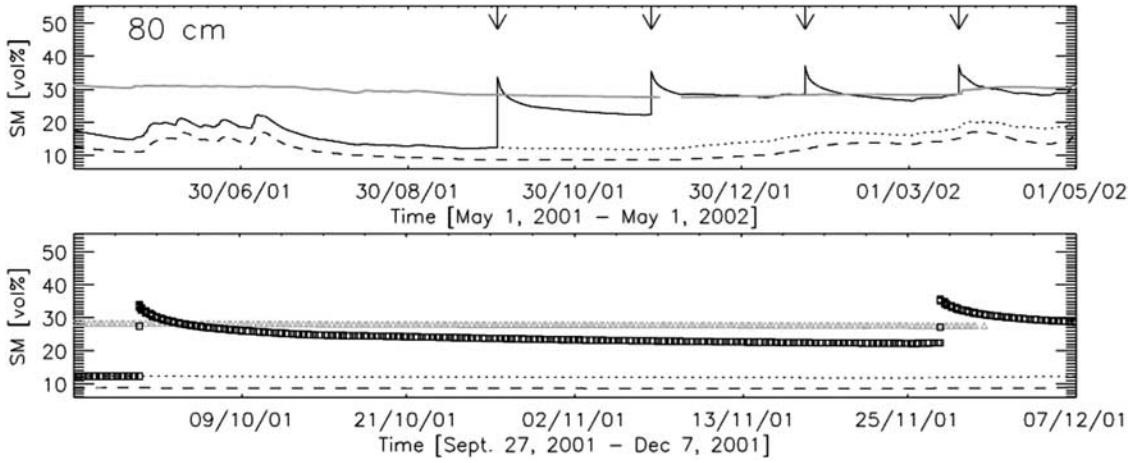

Figure 7. (top) Similar to Figure 3 but only at 80 cm depth and with bias correction (ENBKF). (bottom) Zoom of the first two assimilation steps (squares correspond to the black solid line in Figure 7, top).

previous plots, where experiments with different DA frequencies or DA depths were compared to each other, not to a reference run. V is for the RMSE obtained by the control run validation and P and K stand for the filtering runs. For K runs, only assimilation in a single soil layer was performed, and per K run the results for the different DA depths are shown. For P runs, all available profile data were assimilated. K_1 and P_1 are for assimilation without bias correction, while for K_2 and P_2, bias estimation was included. For the filtering runs, assimilation was performed at a fixed DA frequency of every 8 weeks.

[50] The ensemble mean without filtering (dashed line) was generally worse than the control run (V), which explains that through filtering in 1 layer without bias estimation (K_1), it was difficult to reduce the RMSE below the value for the control run (dotted line), as discussed before. For K_2 the RMSE decreased below the level of the control run for some DA depths, but the spread on the relative values increased. For H probes, assimilation with bias correction yielded better profile estimates after assimilation at any depth. For M probes, it is advised to assimilate in the deepest layers and for L probes it is best to assimilate in the middle layers. Profile assimilation without bias correction (P_1) led to slightly better results than the control run, and with bias correction (P_2) the results improved a lot, mainly for the deeper M and L profiles.

5.2. Innovations

[51] The innovations are the most readily available information to judge if a filter works within its underlying assumptions. If the errors on the observations and on the a priori state estimate would be zero mean, as is assumed in the derivation of the Kalman filter, the innovations should also be distributed around a zero mean for linear systems. For bias-blind state estimation (ENKF, which is also the first stage of the ENBKF), the kth element of the ensemble mean innovation vector is given by $[\mathbf{y}_i - \mathbf{H}_i\tilde{\hat{\mathbf{x}}}_i^-]_k$.

[52] To check the consistency of the innovations with the imposed a priori error covariances and observation error covariances [*Reichle et al.*, 2002a], the ensemble mean innovation for each point in space at each assimilation event was normalized by the imposed $[\mathbf{H}_i\tilde{\mathbf{P}}_{x,i}^-\mathbf{H}_i^T + \mathbf{R}_i]_{kk}$. Figure 11 shows the space-time pdf of all normalized innovations over 25 and 4 assimilation events and for all 24 sensors at 80 cm depth. The mean of the innovations in space and time differed clearly from zero, which reflects the presence of bias in the bias-blind estimates. The spread observed in Figure 11 for the bias-blind state filtering suggests a good consistency, but results from the innovation variability in both space and time. The temporal distributions of the normalized innovations at a single location showed that the imposed spread was chosen larger than necessary for the bias-blind state filtering, which resulted in temporal pdfs with a standard deviation of less than 0.7, mainly in case of intensive assimilations. For the spatial distributions, the standard deviation equaled or exceeded 1. In general, the imposed spread $\tilde{\mathbf{P}}_{x,i}^-$ to represent the uncertainty in the bias-blind forecasts was well chosen for the surface layers (not shown), but could have been reduced in deeper soil layers, especially for more intensive assimila-

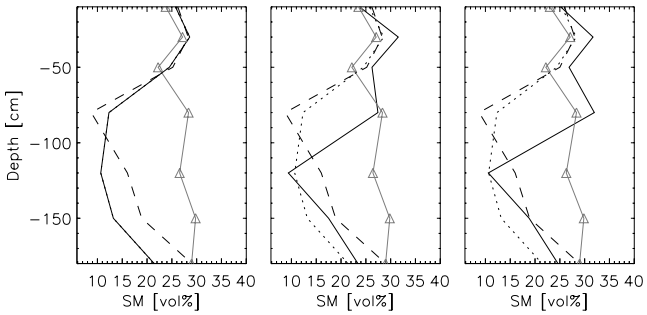

Figure 8. Soil moisture profile at DL3 of observations (triangles), the control run (dashed line), the ensemble mean run without filtering (dotted line), and the ENBKF run (solid line) with assimilation at 80 cm on 2 October 2001 around 1000 LT. Profiles (left) 12 hours before assimilation, (middle) at the assimilation instant, and (right) 12 hours after assimilation.

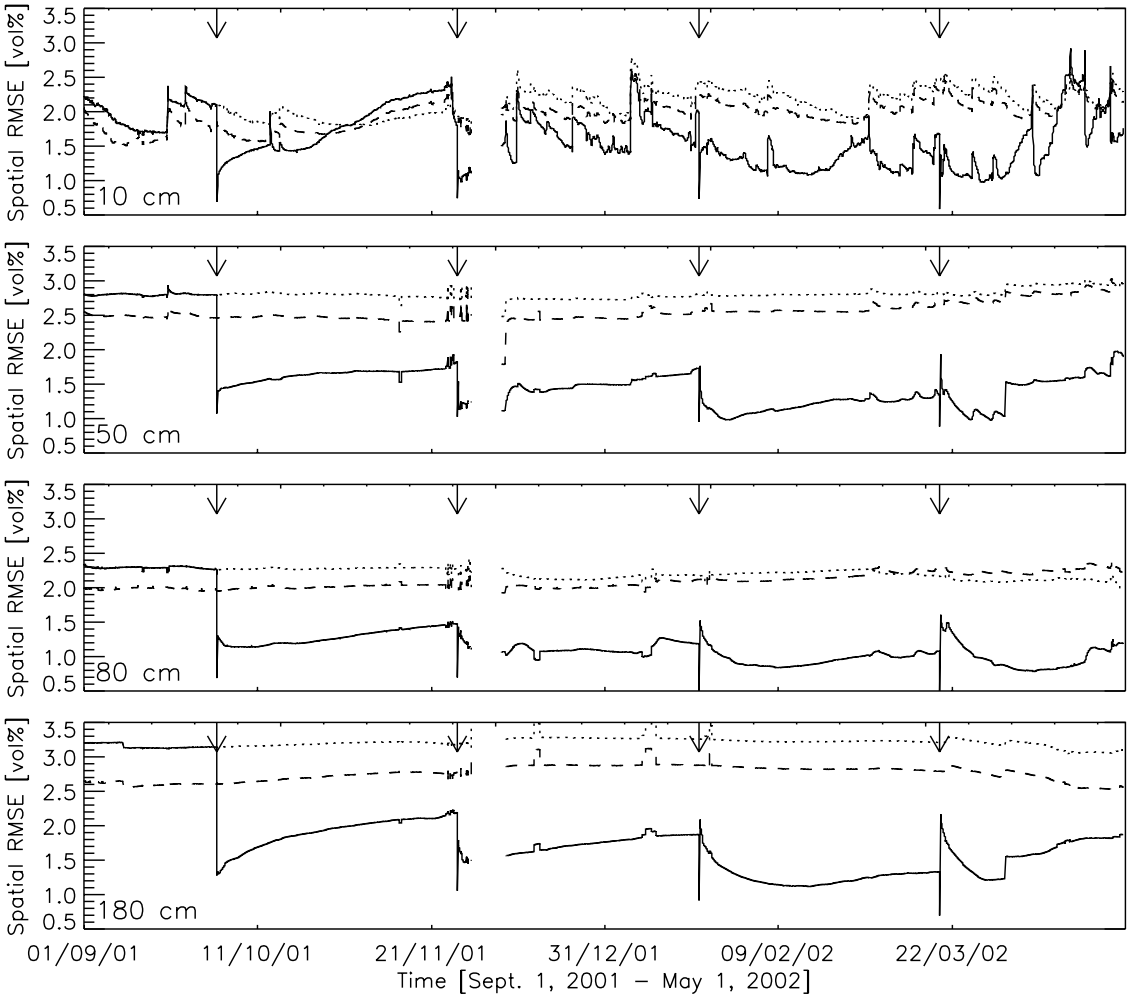

Figure 9. Time series of the root spatial mean square error for the control run (dashed line), the ensemble mean run without filtering (dotted line), and the ENBKF run (solid line) with four assimilation events of complete profiles. The arrows indicate the filtering events. Irregularities are due to variable missing sensors in space.

tions to enlarge the accuracy of the final a posteriori (bias-corrected) state estimate.

6. Conclusions

[53] Soil moisture was estimated for 36 profiles in the OPE^3 field by state and bias estimation through the assimilation of real soil moisture measurements in a nonlinear land surface model by an ensemble Kalman filter. The focus is on the impact of assimilation in several soil layers at different frequencies and on the optimization of the method for a real study, without an in depth evaluation of the effect on related state variables or fluxes, such as evapotranspiration or runoff, which is discussed by De Lannoy et al. (submitted manuscript, 2006).

[54] The performance for state estimation was found to be limited by the presence of model bias. Earlier research [*De Lannoy et al.*, 2006a] had shown that bias was remaining in some layers after calibration of the individual profiles and also that bias was sometimes introduced by ensemble generation. Therefore, in addition to the ENKF for state estimation, a filter for bias estimation was introduced.

[55] For assimilation in a single layer during a fixed time interval, the optimal DA frequency was dependent on the DA depth (both with and without bias estimation). If the assimilation causes adverse effects in layers outside the assimilation layer, e.g., because of bias in the innovations or an incorrect state error covariances, then an intensive assimilation should be avoided. The optimal assimilation depth was generally 80 and 180 cm for the deep M and L profiles, respectively and not determined for shallow H profiles. This was partially a result of the calibration: the model showed more deficiencies for deeper soil layers and hence assimilation has a larger impact. Also, the upper layer soil moisture might have been decoupled from the very complex subsurface soil moisture during considerable periods. This is an unfortunate finding for the estimation of the complex soil moisture profiles, when remote sensing data are used, which generally only provide near-surface soil moisture.

[56] Assimilation of all available data for a profile had most effect on deeper soil profile layers. The impact on the upper layers was only marginal. The optimal assimilation

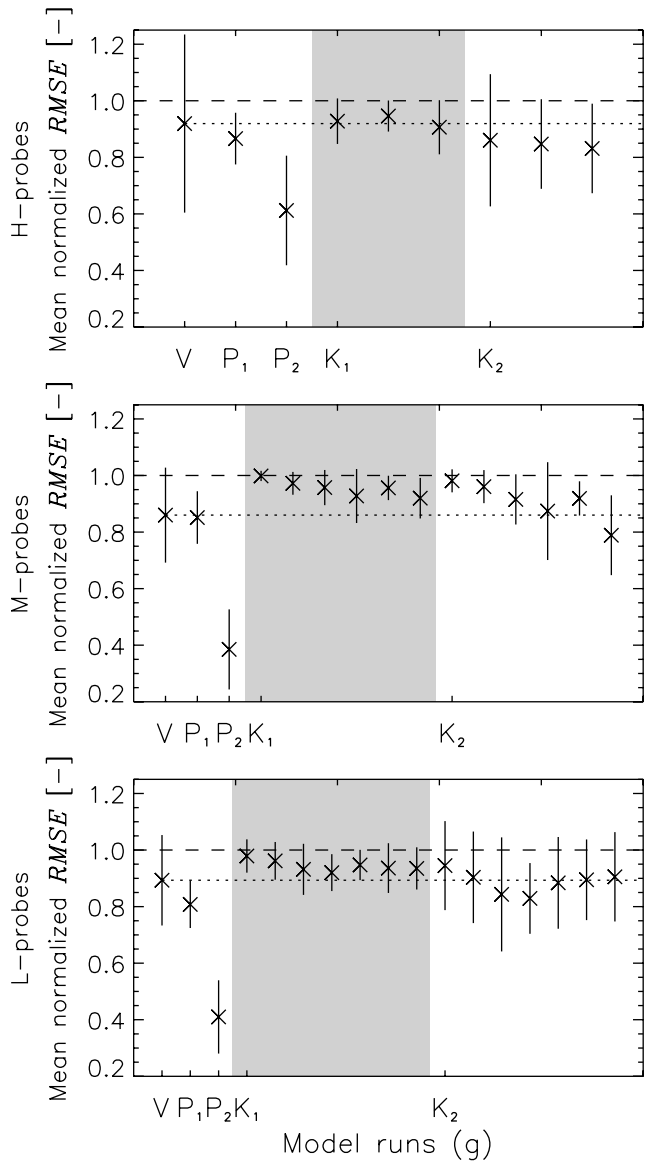

Figure 10. Mean normalized profile-integrated RMSE values for the control run (V), for profile assimilation without and with bias correction (P_1 and P_2, respectively), and for assimilation in a single layer without and with bias correction (K_1 and K_2, respectively). For each type of Kalman filtering, assimilation at the different available depths is shown: for H probes at 10, 30, and 80 cm, for M probes at 10, 30, 50, 120, 150, and 180 cm, and for L probes at 10, 30, 50, 80, 120, 150, and 180 cm. Observations were assimilated with an 8 week interval.

frequency for profile assimilation with bias correction was about 1 to 2 weeks, which is related to the autocorrelation length for soil moisture, and ultimately to the atmospheric forcings. Without bias estimation, there was always a benefit in a more frequent assimilation, while with bias correction, it was possible to greatly reduce the assimilation intensity.

[57] Through the implementation of bias estimation without feedback [*Friedland*, 1969], the overall profile-integrated performance was increased, but this was mostly due to an increased performance in the assimilation layer and less by improvements in surrounding layers. This is due to the zero initialization of the bias vector and the assumed persistence bias model, without any knowledge on the vertical "dynamics" of this bias. It is impossible to estimate the bias in layers for which no observations or knowledge of the truth is available, i.e., the bias system is not observable if not all bias variables in a bias vector are observed. Further, the bias error covariance was assumed proportional to the bias-blind state error covariance, which might reinforce problems encountered in state estimation due to inaccurate estimation of the state error covariance. Also through this method, model overshoots in the state estimation were found. This is because the innovation for the bias-blind analysis contains a bias part and the state correction disappears only slowly, while the bias estimation method assumes that the forecast generated by a bias-blind analysis (the bias correction is not fed back) contains the same bias as was estimated at the analysis step. The advantages and disadvantages of different variants to Friedland's state and bias estimation are further discussed by De Lannoy et al. (submitted manuscript, 2006).

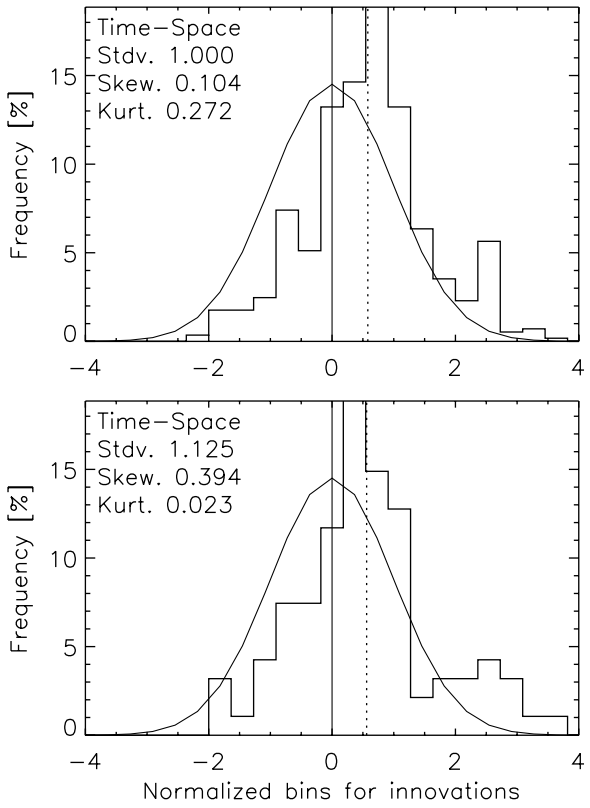

Figure 11. Pdfs of all normalized ensemble mean innovations for all observation locations at 80 cm depth at (top) 25 assimilation events with an interval of 1 week and (bottom) 4 assimilation events with an interval of 8 weeks. The dashed line represents the sample mean. The smooth curve represents the standard normal distribution. "Stdv." stands for standard deviation, "Skew." stands for skewness, and "Kurt." stands for kurtosis.

[58] **Acknowledgments.** The authors thank the Beltsville Agricultural Research Center (BARC), Agricultural Research Service (ARS), USDA, for providing the data. The Hydrological Sciences Branch (HSB) of NASA GSFC is thanked for hosting the first author during part of the research. The authors are very grateful to Rolf Reichle (NASA GSFC/GMAO) for insightful discussions on the filter validation. This research is supported by a Ph.D. fund of the Bijzonder Onderzoeksfonds (BOF) of the Ghent University and by STEREO project SR/00/01 of the Belgian Science Policy (BELSPO). The reviewers are thanked for their suggestions to further improve this paper.

References

Bonan, G. B., S. Levis, L. Kergoat, and K. W. Oleson (2002), Landscapes as patches of plant functional types: An integrating concept for climate and ecosystem models, *Global Biogeochem. Cycles*, *16*(2), 1021, doi:10.1029/2000GB001360.

Boulet, G., Y. Kerr, and A. Chehbouni (2002), Deriving catchment-scale water and energy balance parameters using data assimilation based on extended Kalman filtering, *Hydrol. Sci. J. Sci. Hydrol.*, *47*, 449–467.

Burgers, G., P. J. van Leeuwen, and G. Evensen (1998), On the analysis scheme in the ensemble Kalman filter, *Mon. Weather Rev.*, *126*, 1719–1728.

Crosson, W. L., C. A. Laymon, R. Inguva, and M. P. Schamschula (2002), Assimilating remote sensing data in a surface flux-soil moisture model, *Hydrol. Processes*, *16*, 1645–1662.

Crow, W. (2003), Correcting land surface model predictions for the impact of temporally sparce rainfall rate measurements using an ensemble Kalman filter and surface brightness temperature observations, *J. Hydrometeorol.*, *4*, 960–973.

Crow, W. T., and E. F. Wood (2003), The assimilation of remotely sensed soil brightness temperature imagery into a land surface model using ensemble Kalman filtering: A case study based on ESTAR measurements during SGP97, *Adv. Water Resour.*, *26*, 137–149.

Dai, Y., et al. (2003), The Common Land Model, *Bull. Am. Meteorol. Soc.*, *84*, 1013–1023.

Dee, D. P., and A. M. da Silva (1998), Data assimilation in the presence of forecast bias, *Q. J. R. Meteorol. Soc.*, *124*, 269–295.

Dee, D. P., and R. Todling (2000), Data assimilation in the presence of forecast bias: The GEOS moisture analysis, *Mon. Weather Rev.*, *128*, 3268–3282.

De Lannoy, G. J. M., P. R. Houser, V. R. N. Pauwels, and N. E. C. Verhoest (2006a), Assessment of model uncertainty for soil moisture through ensemble verification, *J. Geophys. Res.*, *111*, D10101, doi:10.1029/2005JD006367.

De Lannoy, G. J. M., N. E. C. Verhoest, P. R. Houser, and T. Gish (2006b), Spatial and temporal characteristics of soil moisture in an intensively monitored agricultural field (OPE^3), *J. Hydrol.*, *331*, 719–730.

Dirmeyer, P. (2000), Using a global soil wetness dataset to improve seasonal climate simulation, *J. Clim.*, *13*, 2900–2921.

Entekhabi, D., H. Nakamura, and E. G. Njoku (1994), Solving the inverse problem for soil moisture and temperature profiles by sequential assimilation of multifrequency remotely sensed observations, *IEEE Trans. Geosci. Remote Sens.*, *32*, 438–448.

Evensen, G. (2003), The Ensemble Kalman filter: Theoretical formulation and practical implementation, *Ocean Dyn.*, *53*, 343–367.

Friedland, B. (1969), Treatment of bias in recursive filtering, *IEEE Trans. Automat. Control*, *14*, 359–367.

Galantowicz, J. F., D. Entekhabi, and E. G. Njoku (1999), Tests of sequential data assimilation for retrieving profile soil moisture and temperature from observed L-band radiobrightness, *IEEE Trans. Geosci. Remote Sens.*, *37*, 1860–1870.

Gish, T., W. Dulaney, K.-J. S. Kung, C. Daughtry, J. Doolittle, and P. Miller (2002), Evaluating use of ground-penetrating radar for identifying subsurface flow pathways, *Soil Sci. Soc. Am. J.*, *66*, 1620–1629.

Heathman, G., P. Starks, L. Ahuja, and T. Jackson (2003), Assimilation of soil moisture to estimate profile soil water content, *J. Hydrol.*, *279*, 1–17.

Hebson, C., and E. Wood (1985), Partitioned state and parameter estimation for real-time flood forecasting, *Appl. Math. Comput.*, *17*, 357–374.

Hoeben, R., and P. A. Troch (2000), Assimilation of active microwave observation data for soil moisture profile estimation, *Water Resour. Res.*, *36*, 2805–2819.

Houser, P. R., W. J. Shuttleworth, J. S. Famiglietti, H. V. Gupta, K. H. Syed, and D. C. Goodrich (1998), Integration of soil moisture remote sensing and hydrologic modeling using data assimilation, *Water Resour. Res.*, *34*, 3405–3420.

Kalman, R. E. (1960), A new approach to linear filtering and prediction problems, *J. Basic Eng.*, *82*, 35–45.

Keppenne, L. C., M. M. Rienecker, N. P. Kurkowski, and D. A. Adamec (2005), Ensemble Kalman filter assimilation of temperature and altimeter data with bias correction and application to seasonal prediction, *Nonlinear Processes Geophys.*, *12*, 491–503.

Koster, R. D., M. Suarez, P. Liu, U. Jambor, A. Berg, M. Kistler, R. Reichle, M. Rodell, and J. Famiglietti (2004), Realistic initialization of land surface states: Impacts on subseasonal forecast skill, *J. Hydrometeorol.*, *5*, 1049–1063.

Margulis, S. A., D. McLaughlin, D. Entekhabi, and S. Dunne (2002), Land data assimilation of soil moisture using measurements from the Southern Great Plains 1997 Field Experiment, *Water Resour. Res.*, *38*(12), 1299, doi:10.1029/2001WR001114.

Maybeck, P.S. (1979). *Stochastic Models, Estimation, and Control*, *Math. Sci. Eng.*, vol. 141, Elsevier, New York.

McPherson, R. D. (1975), Progress, problems, and prospects in meteorological data assimilation, *Bull. Am. Meteorol. Soc.*, *56*, 1154–1166.

Moradkhani, H., S. Sorooshian, H. V. Gupta, and P. R. Houser (2005), Dual state-parameter estimation of hydrological models using ensemble Kalman filter, *Adv. Water Resour.*, *28*, 135–147.

Ni-Meister, W., J. Walker, and P. R. Houser (2005), Soil moisture initialization for climate prediction: Characterization of model and observation errors, *J. Geophys. Res.*, *110*, D13111, doi:10.1029/2004JD005745.

Paltineanu, I. C., and J. Starr (1997), Real-time soil water dynamics using capacitance probes: Laboratory calibration, *Soil Sci. Soc. Am. J.*, *61*, 1576–1585.

Pauwels, V. R. N., R. Hoeben, N. E. C. Verhoest, F. P. De Troch, and P. A. Troch (2002), Improvement of TOPLATS-based discharge predictions through assimilation of ERS-based remotely sensed soil moisture values, *Hydrol. Processes*, *16*, 995–1013.

Reichle, R. H., and R. Koster (2003), Assessing the impact of horizontal error correlations in background fields on soil moisture estimation, *J. Hydrometeorol.*, *4*, 1229–1242.

Reichle, R. H., and R. Koster (2005), Global assimilation of satellite surface soil moisture retrievals into the NASA catchment land surface model, *Geophys. Res. Lett.*, *32*, L02404, doi:10.1029/2004GL021700.

Reichle, R. H., D. B. McLaughlin, and D. Entekhabi (2002a), Hydrologic data assimilation with the ensemble Kalman filter, *Mon. Weather Rev.*, *120*, 103–114.

Reichle, R. H., J. P. Walker, P. R. Houser, and R. D. Koster (2002b), Extended versus ensemble Kalman filtering for land data assimilation, *J. Hydrometeorol.*, *3*, 728–740.

Reichle, R. H., R. Koster, J. Dong, and A. Berg (2004), Global soil moisture from satellite observations, land surface models, and ground data: Implications for data assimilation, *J. Hydrometeorol.*, *5*, 430–442.

Vrugt, J. A., C. G. H. Diks, H. V. Gupta, W. Bouten, and J. M. Verstaten (2005), Improved treatment of uncertainty in hydrologic modelling: Combining the strengths of global optimization and data assimilation, *Water Resour. Res.*, *41*, W01017, doi:10.1029/2004WR003059.

Walker, J. P., and P. R. Houser (2004), Requirements of a global near-surface soil moisture satellite mission: Accuracy, repeat time, and spatial resolution, *Adv. Water Resour.*, *27*, 785–801.

Walker, J. P., G. R. Willgoose, and J. D. Kalma (2001a), One-dimensional soil moisture profile retrieval by assimilation of near-surface observations: A comparison of retrieval algorithms, *Adv. Water Resour.*, *24*, 631–650.

Walker, J. P., G. R. Willgoose, and J. D. Kalma (2001b), One-dimensional soil moisture profile retrieval by assimilation of near-surface measurements: A simplified soil moisture model and field application, *J. Hydrometeorol.*, *2*, 356–373.

G. J. M. De Lannoy, V. R. N. Pauwels, and N. E. C. Verhoest, Laboratory of Hydrology and Water Management, Ghent University, Coupure links 653, B-9000 Ghent, Belgium. (gabrielle.delannoy@ugent.be)

P. R. Houser, Center for Research on Environment and Water, George Mason University, 4041 Powder Mill Road, Suite 302, Calverton, MD 20705-3106, USA.